Journal of Power Sources 266 (2014) 79–87

Contents lists available at ScienceDirect

Journal of Power Sources

journal homepage: www.elsevier.com/locate/jpowsour

Short communication

Application of sol–gel technique to synthesis of copper–cobalt spinel on the ferritic stainless steel used for solid oxide fuel cell interconnects

Pouyan Paknahad, Masoud Askari*, Milad Ghorbanzadeh

Department of Materials Science and Engineering, Sharif University of Technology, Azadi Avenue, P.O. Box 11155-9466, Tehran, Iran

HIGHLIGHTS

- Cu–Co spinel layer was deposited on AISI 430 by sol–gel dip-coating process.
- $CuCo_2O_4$ coating greatly improves the oxidation resistance of AISI 430 alloy.
- $CuCo_2O_4$ layer has an acceptable conductivity and long-term stability during oxidation.
- Applied coating acted as an effective barrier to Cr outward diffusion.

ARTICLE INFO

Article history:
Received 17 March 2014
Received in revised form
17 April 2014
Accepted 23 April 2014
Available online 13 May 2014

Keywords:
Solid oxide fuel cell
Metallic interconnects
Spinel
Coating
Sol–gel

ABSTRACT

The conductive $CuCo_2O_4$ spinel coating is applied on the surface of the AISI 430 ferritic stainless steel by the dip-coating sol–gel process and it is evaluated in terms of the microstructure, oxidation resistance and electrical conductivity. The results show that the $CuCO_2O_4$ coating forms a double-layer scale consisting of a Cr, Fe-rich subscale and Cu–Co spinel top layer after 500 h in air at 800 °C. This scale is protective, acts as an effective barrier against Cr migration into the outer oxide layer and alleviates the cathode Cr-poisoning. The oxidation resistance is significantly enhanced by the protective coating with a parabolic rate constant of 5.8×10^{-13} $gr^2\ cm^{-4}\ s^{-1}$, meanwhile the electrical conductivity is considerably improved due to inhibited growth of resistive Cr_2O_3 oxide scale. The area specific resistance at temperatures between 550 and 800 °C is in the range of 11.5 and 22.2 mΩ cm^2.

1. Introduction

Fuel cells are the green energy conversion equipments which convert fuels directly into electricity. Due to low environmental impact and high efficiency, they may play an important role in future clean energy generation. Nonetheless, high cost is still an important obstacle to the commercialization of this technology. Because of higher energy conversion efficiency and excellent fuel flexibility, solid oxide fuel cells (SOFC) have received the most attraction among the various kinds of fuel cells. So, development of less expensive materials and simpler manufacturing processes for SOFC components is required [1].

Interconnect is a critical component of the SOFC that physically separates the oxidant and fuel gases, distributes the gases to electrodes and provides electrical connections between single stacks. Because of the high operating temperature, requirements for the interconnect materials, such as high temperature oxidation resistance, high electrical conductivity and thermal expansion compatibility with other cell components are essentially stringent [2–4].

Ferritic stainless steel alloys as interconnects have attracted more attention due to their low raw materials cost, excellent formability, relatively higher toughness and mechanical strength, and higher electrical and thermal conductivities compared to traditional ceramic alternatives. Nevertheless, they have low resistance against Cr_2O_3 evaporation in the SOFC operation environment. The volatile chromium species such as CrO_3 and $CrO_2(OH)_2$ can contaminate the cathode and cause rapid degradation of cell performance [1–12].

* Corresponding author. Tel.: +98 21 6616 5206; fax: +98 21 6600 5717.
E-mail addresses: Paknahad@mehr.sharif.ir (P. Paknahad), askari@sharif.edu, pouyanpaknahad@yahoo.com (M. Askari).

http://dx.doi.org/10.1016/j.jpowsour.2014.04.122
0378-7753/

One of the most effective approaches to improve the ferritic stainless steel interconnect performance is to apply a surface coating to enhance conductivity and reduce oxide scale growth and Cr volatility. Generally, spinels can serve as barriers to Cr cation migration and possess high electronic conductivity; therefore, spinels that contain no Cr are favored for the coating application to meet all the requirements [2,3,13–21]. Investigations show that cobalt spinels usually have the lowest thermal expansion coefficient (TEC) and the highest thermal stability between room temperature and 900 °C. The cobaltite conductivity can be improved by the presence of manganese and/or copper elements because of their multiple valence states [22].

In this study, Cu–Co spinel coating was applied on the surface of the AISI 430 ferritic stainless steel by using a cost-effective sol–gel dip-coating process that is readily applicable to metallic interconnects with various shapes. Oxidation kinetics, growth of oxide scale and area specific resistance of coated and uncoated AISI 430 were evaluated.

2. Experimental

2.1. Specimen preparation

Commercial ferritic stainless steel AISI 430 (Hardox) was used as substrate. The chemical composition of the alloy is listed in Table 1. The sheet was cut into pieces with dimensions of 10 × 10 × 1 mm coupons and each piece was polished. The polished substrates were ultrasonically washed in with distilled water and acetone for 10 min, rinsed in water and alcohol and finally dried in oven at 100 °C.

The sol–gel solution for applying Cu–Co spinel (nominal $CuCo_2O_4$) coating was prepared by using proportional amounts of copper nitrate tri-hydrate ($Cu(NO_3)_2 \cdot 3H_2O$), cobalt nitrate hexahydrate ($Co(NO_3)_2 \cdot 6H_2O$), acid citric monohydrate and ethylene glycol. Dip-coating process was utilized to coat the solution on the surface of the prepared samples. A group of coated samples were heated in a reducing atmosphere (5% H_2 + Ar) for 2 h at 800 °C and then exposed to 800 °C air for another 2 h, these are termed the “pre-reduced” samples. Other group of samples were heated in an oxidizing atmosphere for 2 h at 800 °C, these are termed the “pre-oxidized” samples. Reducing atmosphere was employed to alleviate substrate oxidation during the formation of the spinel coating and improve the interface adhesion [2,3,6,20].

2.2. Measurements and characterization

The oxidation kinetics of coated and uncoated steel coupons was investigated by performing cyclic oxidation tests in stagnant air. The samples were oxidized at 800 °C in air for 50 h and then cooled to room temperature, This procedure was repeated 10 times. The oxidation weight gain of each sample after every cyclic test was measured by using a GD503 electronic balance with an accuracy of 10^{-4} gr.

Electrical resistance measurements of the samples were performed using a DC two-probe, four-point technique. Area specific resistance (ASR) of the uncoated and spinel-coated samples was investigated as a function of time at 800 °C for 500 h (isothermal oxidation). To reduce the ohmic resistance, the silver mesh was

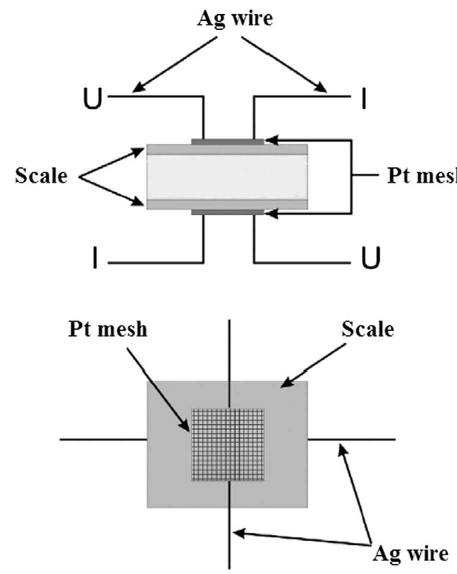

Fig. 1. Schematic diagram of the ASR measurement setup utilizing the DC two-probe four-point method.

installed on both sides of the samples by silver paste. A constant current of 200 mA was passed through two silver wires and the voltage was recorded every 30 min. The data were used to calculate the resistance and ASR. The effect of temperature on the ASR of oxidized samples (for 500 h) was investigated in the range of 550–800 °C. Fig. 1 shows a schematic diagram of the setup used for the measurement of the ASR.

The crystal structure of the coating was analyzed by X-ray diffraction (XRD) method using a Philips X'pert MPD diffractometer with Cu-kα radiation. Microstructure and elemental analysis of the samples were investigated using field-emission scanning electron microscope (FE-SEM, TESCAN model MIRA3 LM) with an energy dispersive X-ray (EDX) analyzer.

To examine whether $CuCo_2O_4$ can be used as a conductive coating material for ferritic stainless steel, the TEC and electrical conductivity of spinel were measured. To investigate these parameters, rectangular bulk sample of $CuCo_2O_4$ spinel was prepared and sintered at 1100 °C for 4 h. The size of the sample was 5 × 6 × 25 mm. TEC measurement was done by using an NETZSCH DIL 402 dilatometer from room temperature up to 800 °C. The electrical conductivity was measured by the standard DC four-point technique from 500 to 800 °C.

3. Results and discussion

3.1. Electrical conductivity and TEC of $CuCo_2O_4$

Fig. 2 shows the thermal expansion curve, from which the TEC of the sample was calculated. Over the temperature range of 25–800 °C, the TEC of $CuCo_2O_4$ is $11.4 \times 10^{-6}\ K^{-1}$ which is very close to the TEC of ferritic stainless steel ($\sim 12 \times 10^{-6}\ K^{-1}$). The temperature dependence of the electrical conductivity, σ for the $CuCo_2O_4$ spinel in air is shown in Fig. 3. The conductivity of the spinel is 15.2 and

Table 1
Chemical composition of the AISI 430 alloy.

Elements	Fe	Cr	Mn	Cu	Co	Ni	Mo	Al	Si	C	S	V
Weight percent	81.65	17.55	0.25	0.13	0.05	0.127	0.019	0.015	0.15	0.046	0.001	0.012

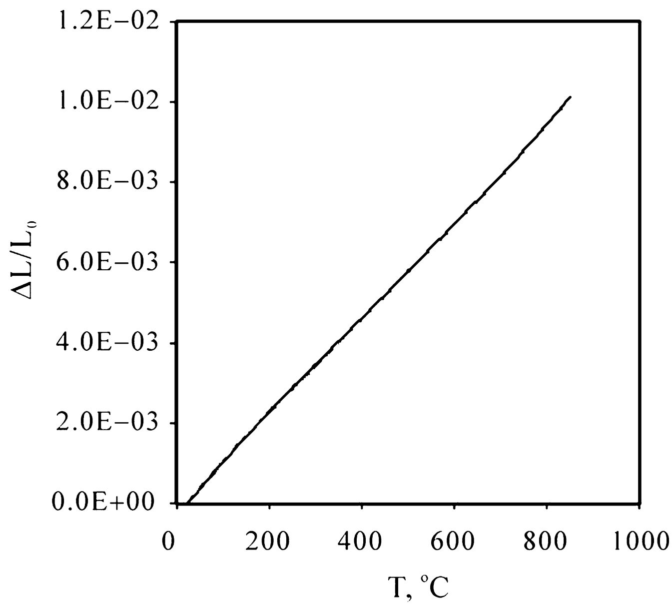

Fig. 2. Thermal expansion of $CuCo_2O_4$ bulk sample measured from room temperature to 800 °C.

27.5 S cm^{-1} at 500 and 800 °C, respectively. Although, these results are more desirable compared to other reported results, but they are still lower than those obtained for $(Cu, Mn)_3O_4$ and $(Co, Mn)_3O_4$ spinels [22]. However, it is acceptable for the metallic interconnect protection layer, which is usually relatively thin, within 1–50 μm in thickness. There is a linear relationship between $\ln(\sigma T)$ and $1/T$, therefore the activation energy (E) of the bulk sample can be calculated according to the following equation

$$\sigma T = \mathrm{k} \exp\left(\frac{-E}{RT}\right) \tag{1}$$

where R is the gas constant and k is a constant that depends on sample properties [1].

Apparently, both electrical conductivity and TEC results reveal that $CuCo_2O_4$ spinel is potentially suitable to be used as an alternative protection coating for SOFC metallic interconnects.

3.2. Structural and microstructural properties of coating

Fig. 4 shows the XRD pattern of the pre-reduced as-coated AISI 430 alloy coupon before oxidation test. Other than the signals from the substrate, $CuCo_2O_4$ and Cr_2O_3 phases were detected, which reveal that the AISI 430 alloy was oxidized during the heat treatment for coating development.

Fig. 5(a) and (c) represents the surface morphologies of "pre-reduced" and "pre-oxidized" samples, respectively. The application of reducing atmosphere pre-treatment significantly affects the morphology and structure of the spinel coatings. Using a reducing atmosphere leads to formation of a uniform, dense and crack-free surface structure, while many cracks and holes exist on the surface of the "pre-oxidized" sample. This indicates that the reducing atmosphere is a possible solution to prevent the cracking and spallation of the applied coating. These results are consistent with the previous reported data [2,3,6,20]. The EDS results of "pre-reduced" and "pre-oxidized" surfaces (Fig. 5(b) and (d) respectively) show that the outmost scale is rich in Cu and Co for both samples.

Fig. 6 demonstrates the cross-sectional morphology and the EDS line scan of the "pre-reduced" as-coated AISI 430 alloy. A homogeneous and dense oxide layer, approximately 8 μm thick, was formed on the substrate. The EDS analysis (Fig. 6(b)) shows that the outer oxide layer contains primarily Cu and Co, and the inner oxide layer mainly consists of Cr, so these layers are made of $CuCo_2O_4$ and Cr_2O_3, respectively.

The cross-section morphology and corresponding EDS line scan of the uncoated and "pre-reduced" as-coated AISI 430 alloy cyclically oxidized at 800 °C in air for up to 500 h are shown in Figs. 7 and 8. For the uncoated sample, thickness of the oxide scale is about 12 μm. The EDS line scan profile in Fig. 7(b) indicates that the scale is comprised a Cr-rich inner layer adjacent to the alloy substrate and a Fe-rich outer layer, suggesting a fast outward diffusion of Fe from the substrate into the scale. Formation of porosity at the interface of the Fe-rich and Cr-rich layers (Fig. 7(a)) is attributed to

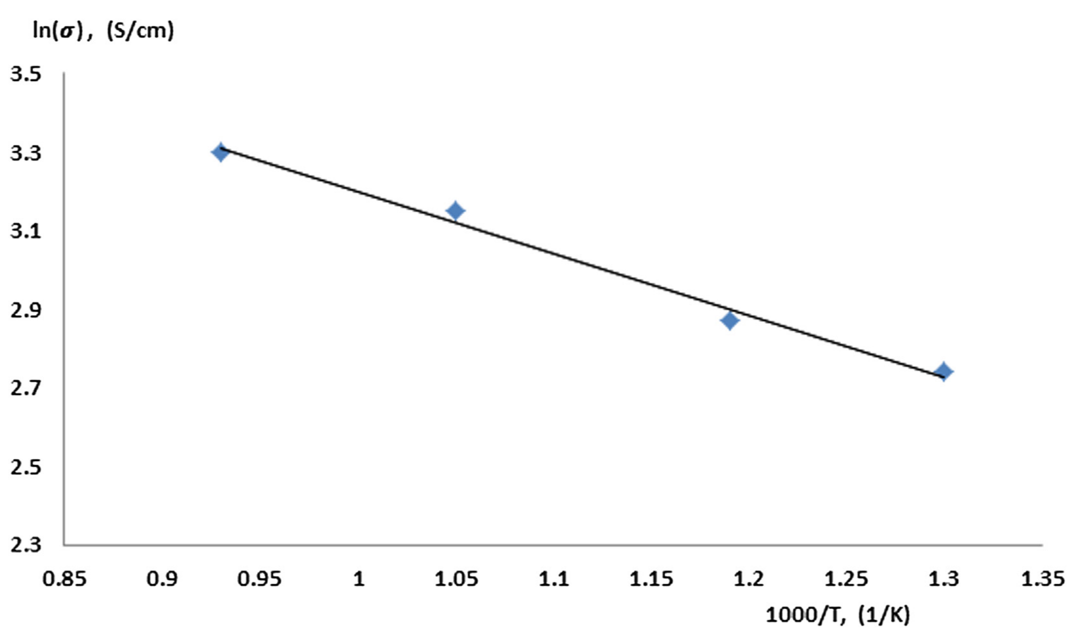

Fig. 3. Arrhenius plot of the electrical conductivity of $CuCo_2O_4$ from 500 to 800 °C.

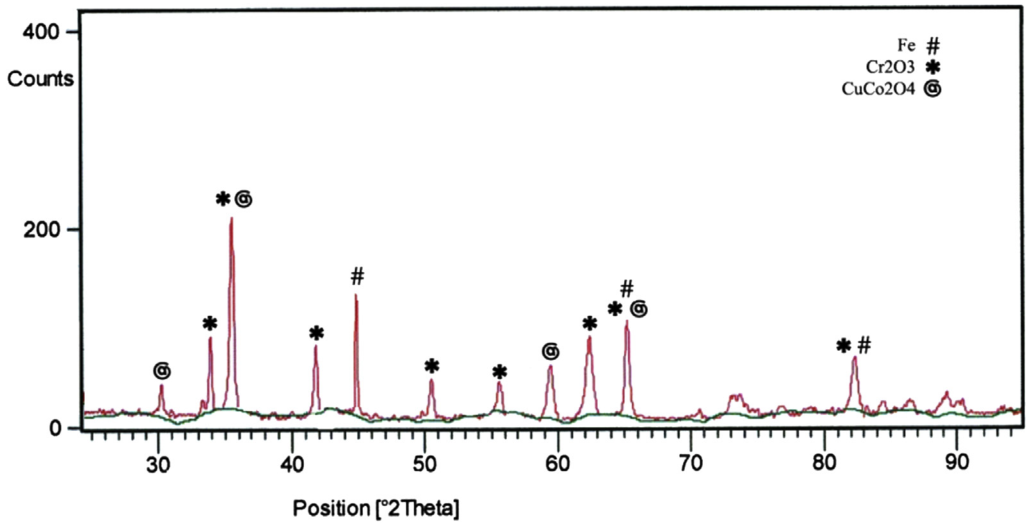

Fig. 4. XRD pattern of the pre-reduced as-coated AISI 430 alloy after heat treatment.

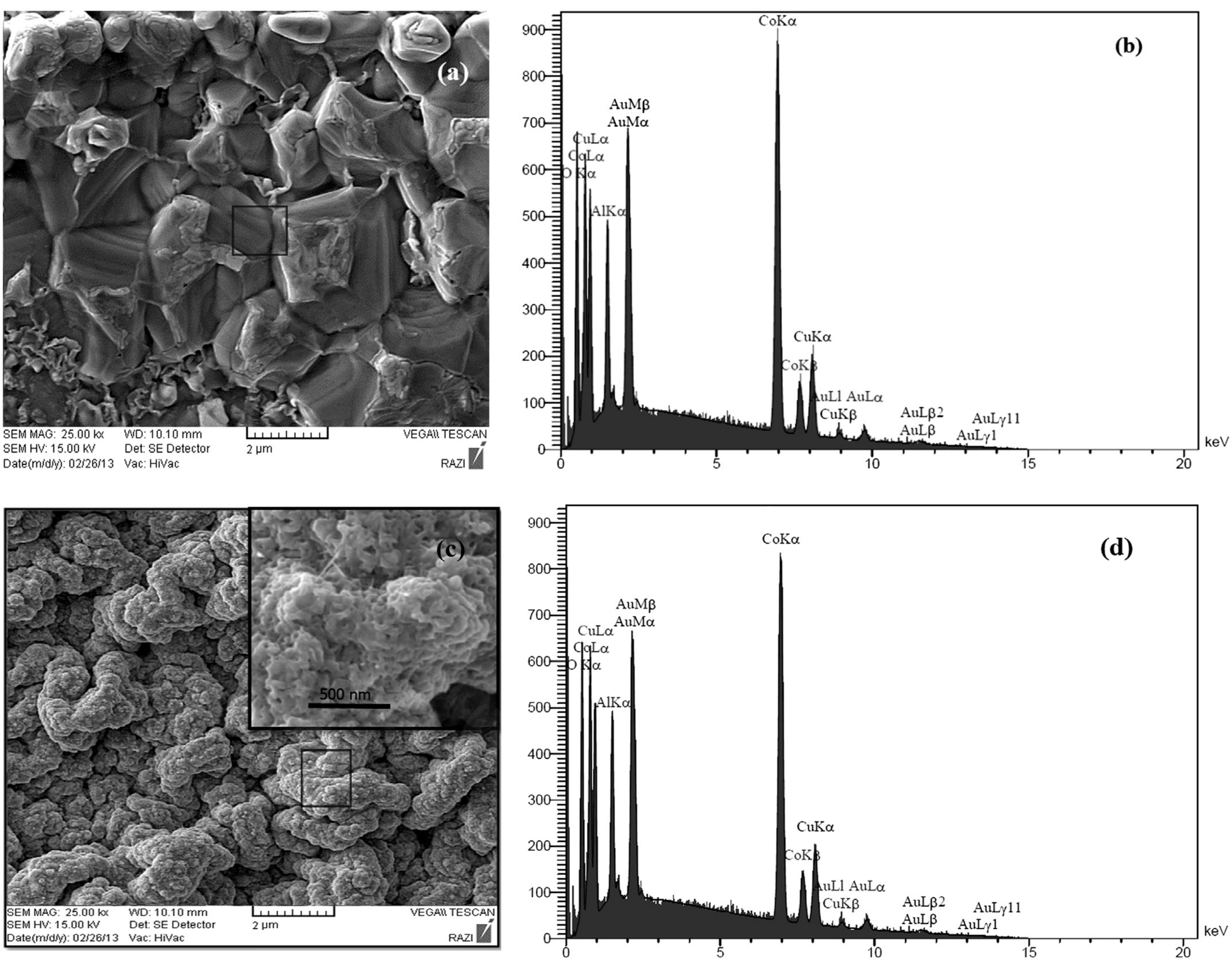

Fig. 5. Surface morphology (a), EDS result (b) of "pre-reduced", and surface morphology (c), EDS result (d) of "pre-oxidized" Cu–Co spinel-coated AISI 430 alloy.

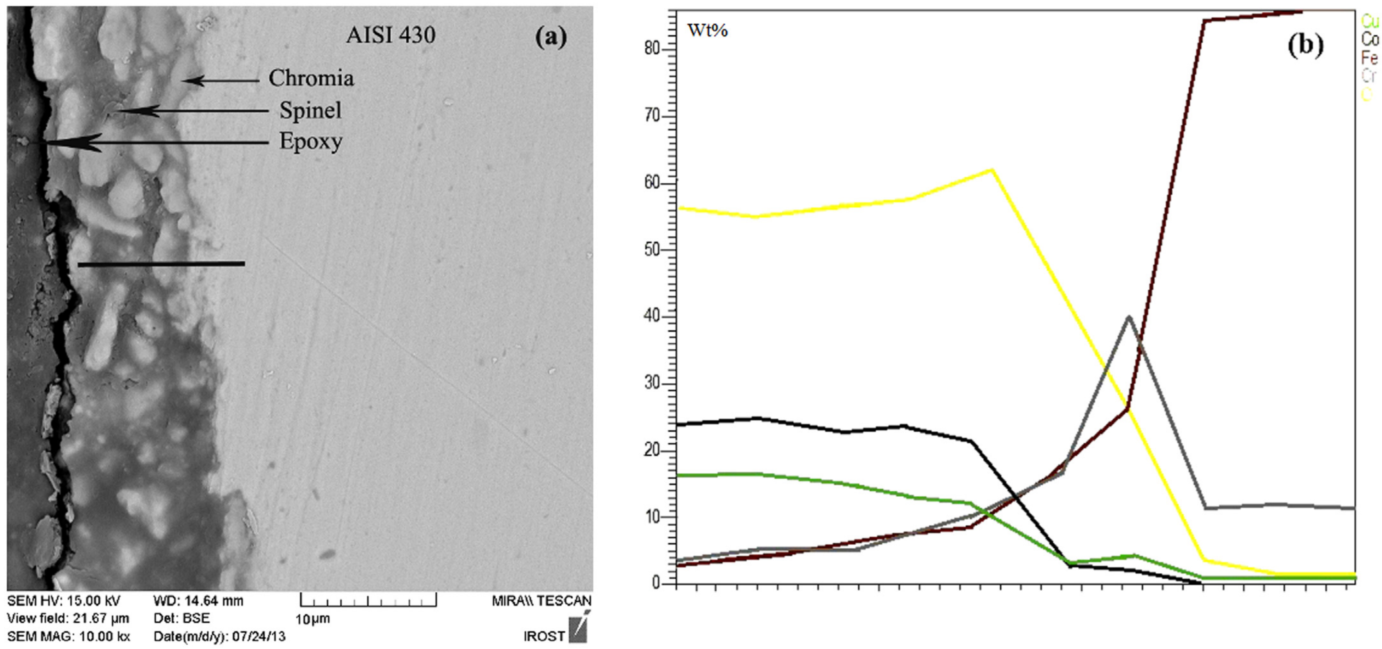

Fig. 6. Cross-sectional backscattered electron microstructure (a) and EDS line scan profile (b) of the "pre-reduced" $CuCo_2O_4$-coated AISI 430.

the large TEC difference between oxide layers, and inward diffusion of the oxygen ions through the Fe-rich phase [15,22–25]. In the case of the spinel-coated sample (Fig. 8), the oxide scale is rich in Cr and Fe in the regions close to the substrate. The coated layer was dense and uniform in thickness (about 8 μm) and also it showed complete adherence to the scale. In addition, no crack and spallation were observed in the coating which is due to nearly similar thermal properties of the oxide scale and the coating.

Based on the above results, it can be concluded that the formed coating via sol–gel process is relatively dense and thermally stable in oxidizing atmosphere. This coating is effective on suppressing the outward diffusion of Cr and inward diffusion of oxygen, which is expected to significantly reduce the oxidation kinetics and alleviate the cathode Cr-poisoning.

3.3. Oxidation kinetics

Fig. 9 illustrates the specific weight gain as a function of time for uncoated and "pre-reduced" as-coated steel coupons. The oxidation rate for uncoated sample is remarkably higher than coated one, this is due to the bare substrate in uncoated samples, which oxidizes freely. In both of the samples, weight gain increased parabolically

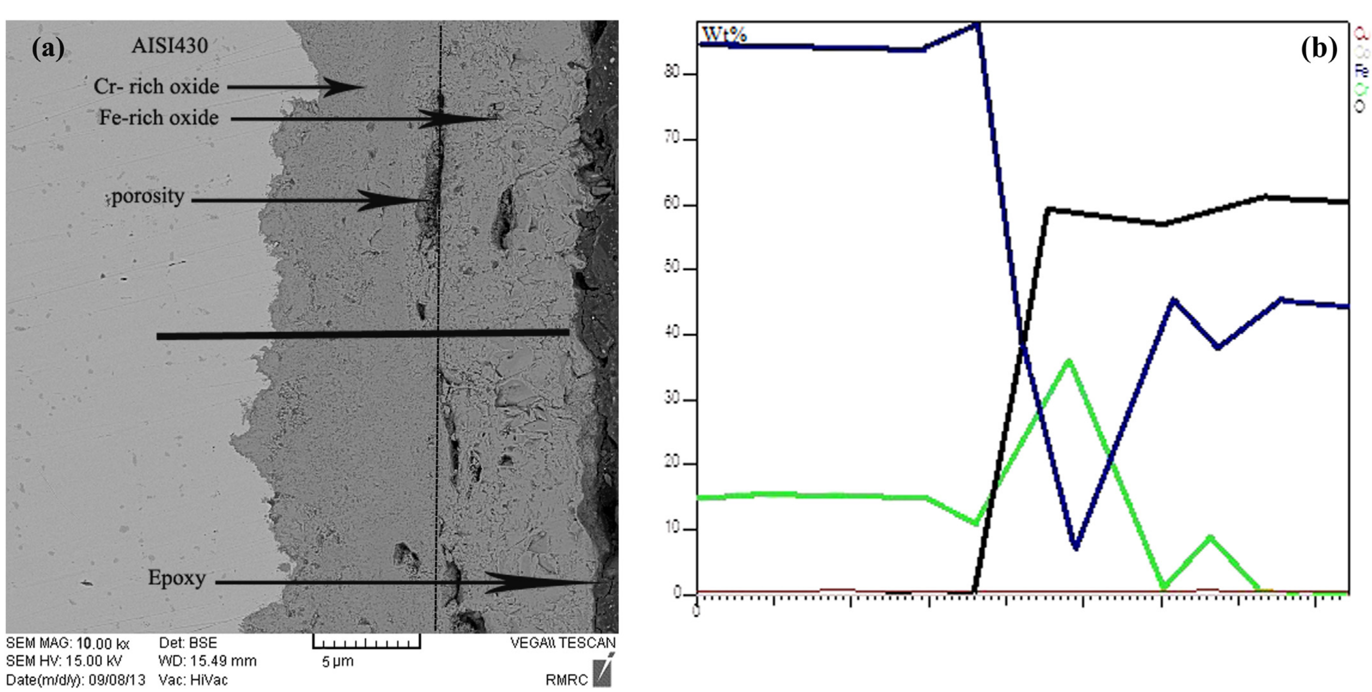

Fig. 7. Cross-section microstructure (a) and EDS line scan profile (b) of the uncoated AISI 430 alloy cyclically oxidized at 800 °C in air for 500 h.

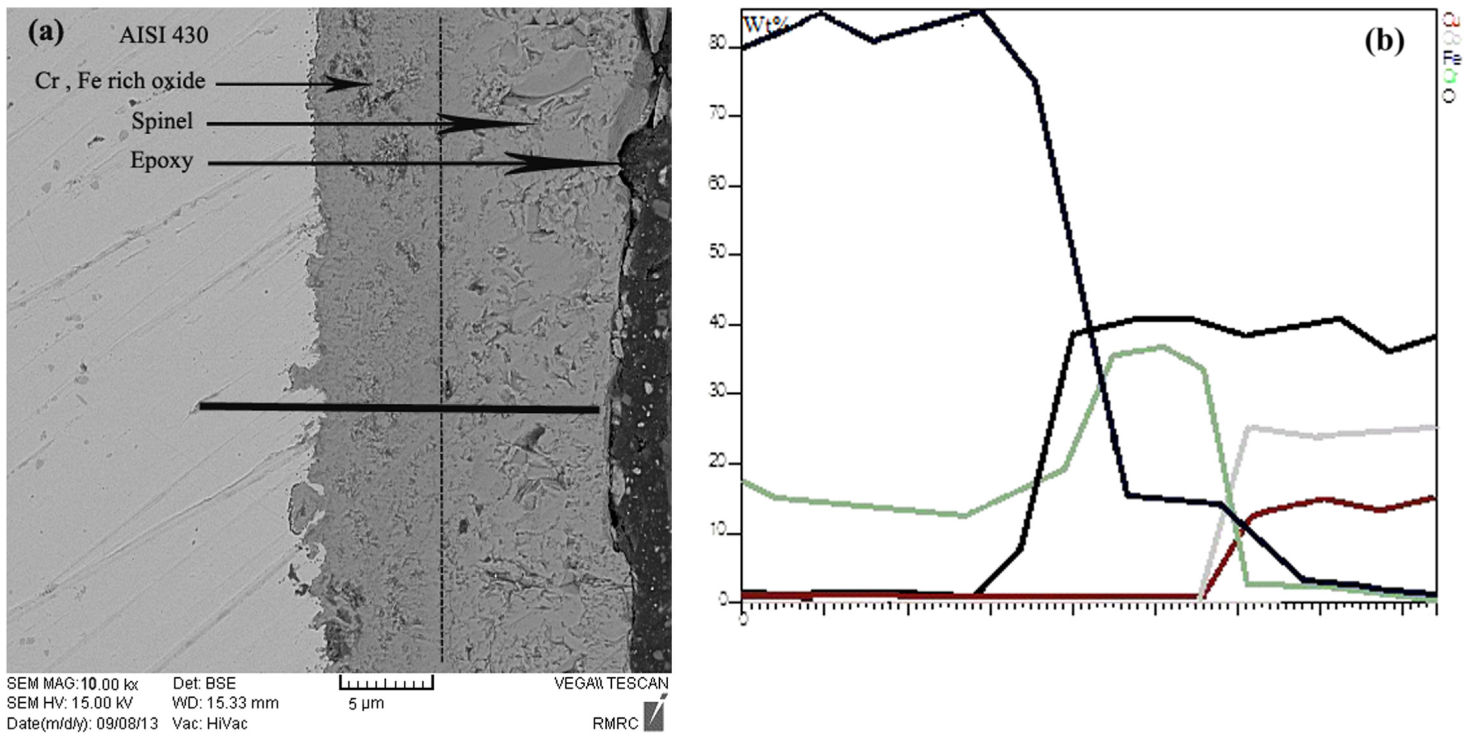

Fig. 8. Cross-section microstructure (a) and EDS line scan profile (b) of the $CuCo_2O_4$ spinel-coated AISI 430 alloy cyclically oxidized at 800 °C in air for 500 h.

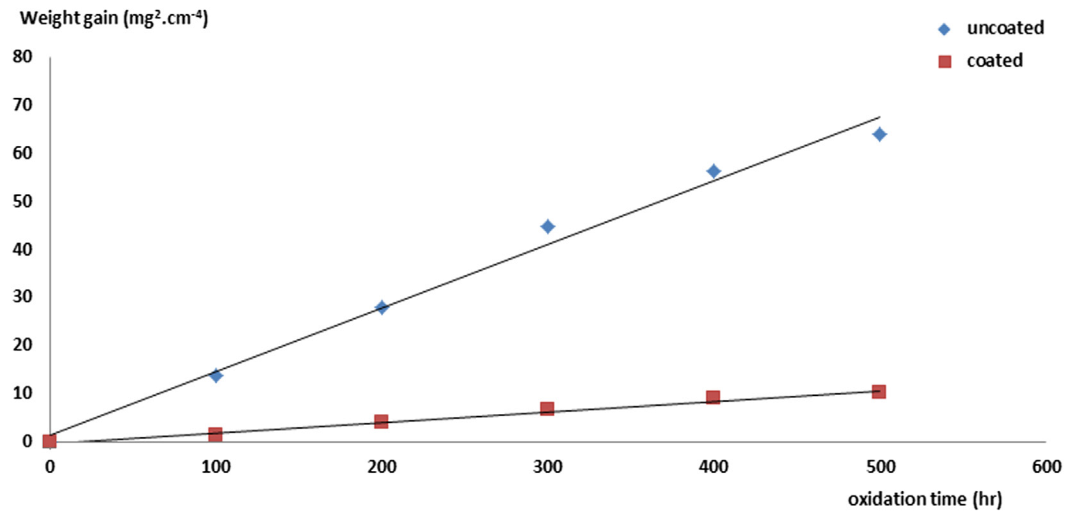

Fig. 9. Oxidation weight gain of the $CuCo_2O_4$-coated AISI 430 alloy as a function of cyclic oxidation time at 800 °C in air, in comparison with the uncoated AISI 430 alloy.

with the isothermal oxidation, satisfying the parabolic kinetics law described by

$$\left(\frac{\Delta W}{A}\right)^2 = \mathrm{K}\,t \quad (2)$$

where ΔW is the weight gain (gr), A is the sample surface area (cm^2), K is the parabolic rate constant ($gr^2\ cm^{-4}\ s^{-1}$) and t is the oxidation time (h). The experimentally obtained K of the $CuCo_2O_4$-coated AISI 430 alloy is $5.8 \times 10^{-13}\ gr^2\ cm^{-4}\ s^{-1}$, which is significantly lower than that of the uncoated alloy, $K = 3.6 \times 10^{-11}\ gr^2\ cm^{-4}\ s^{-1}$. The bare substrate had a weight change of 8 mg cm^{-2} after 500 h isothermal oxidation, while the coated sample had a weight change of 3.2 mg cm^{-2}. Resulted K for $CuCo_2O_4$-coated is lower than the one obtained for $MnCo_2O_4$ [1], $NiCo_2O_4$ [3], $LaCrO_3$ and $La_{0.8}Sr_{0.2}CrO_3$ [8] -coated stainless steel. It can be seen that the oxidation of AISI 430 alloy effectively decreased by application of the $CuCo_2O_4$ spinel coating. Previous studies [1–3,5,6,8] have confirmed that the oxidation kinetics of the both samples is controlled by the cations outward diffusion and the anions inward diffusion.

3.4. ASR evaluation

One of the critical requirements for metallic interconnect materials is a relatively low and stable electrical resistance during SOFC operation. The area specific resistance (ASR, mΩ cm^2), which represents both the electrical conductivity and thickness of the oxide scale, is conventionally adopted as a measure of the electrical performance of the interconnect [3].

3.4.1. ASR evaluation as a function of time

The area specific resistance for the uncoated and coated AISI 430 stainless steel, as a function of time, is plotted in Fig. 10. It can be seen that the bare AISI 430 alloy represents a pronounced increase in ASR from 1 mΩ cm^2 to 33.5 mΩ cm^2 over 500 h. However, the ASR increase is about 11 mΩ cm^2 and no obvious degradation is observed for the coated alloy after operated at 800 °C for 500 h. ASR values for the uncoated AISI 430 increase rapidly with oxidation

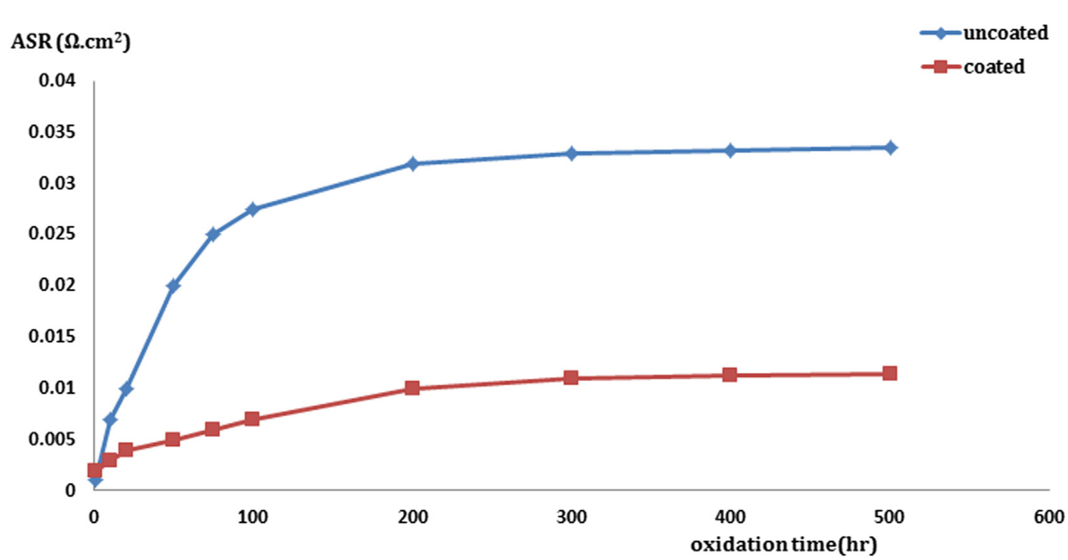

Fig. 10. ASR values for $CuCo_2O_4$-coated and uncoated AISI 430 stainless steel at 800 °C in air as a function of time.

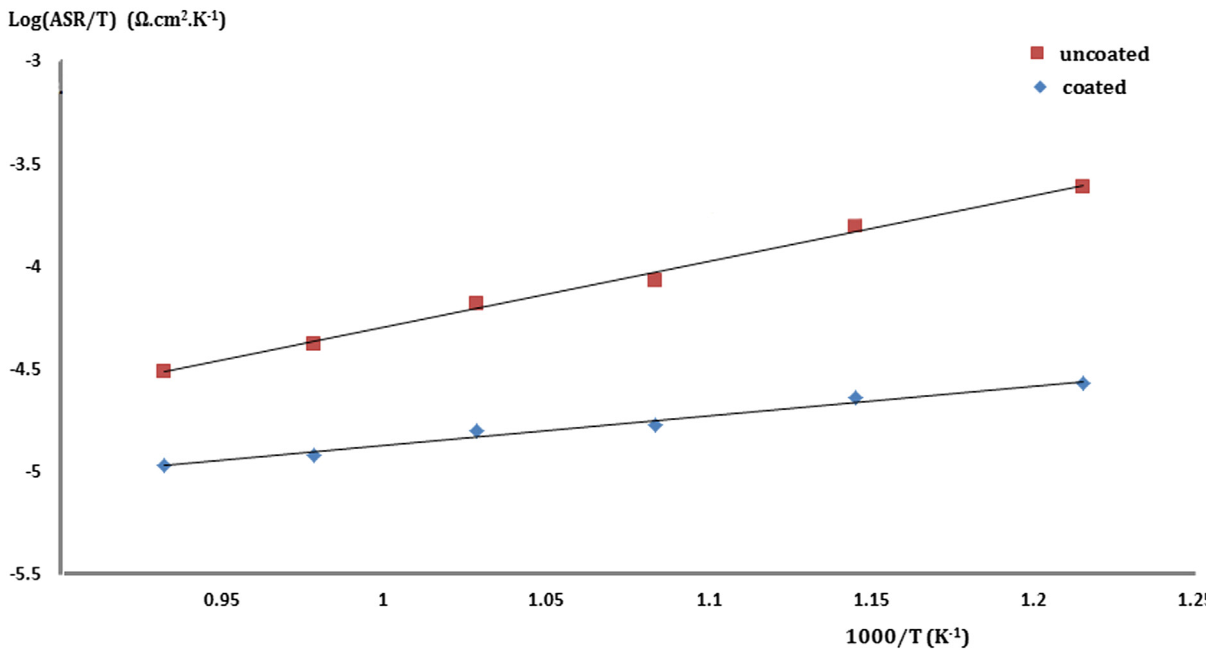

Fig. 11. Area specific resistance of the uncoated and $CuCo_2O_4$-coated AISI 430 as a function of temperature after cyclically oxidation test in air at 800 °C for 500 h.

time for up to 100 h and approach a constant value (33 mΩ cm^2) after about 300 h. The $CuCo_2O_4$-coated specimen, however shows a very low resistance for up to 200 h of oxidation and no further increase in ASR is seen for the test time of 500 h. The slope of diagram decreases with oxidation time increase. This behavior is well consistent with the weight gain behavior of samples and further demonstrates the acceptable oxidation resistance of $CuCo_2O_4$-coated alloy. The resulted ASR is lower than the one obtained for $Mn_{0.9}Y_{0.1}Co_2O_4$ [7], LSM [26], $(La,Sr)CrO_3$ [27] and $MnCo_2O_4$ [28] -coated ferritic stainless steel. Several factors can contribute to the improved electronic conductivity for the $CuCo_2O_4$-coated specimen over uncoated AISI 430 steel. These include the higher electrical conductivity of the scale consisting of Cu–Co containing spinel layer, improved adhesion of the scale to the substrate and elimination of scale spallation [3,20].

3.4.2. ASR evaluation as a function of temperature

To investigate the effect of temperature on the area specific resistance, the ASR was measured at different temperatures (from 550 to 800 °C) for coated and uncoated samples after pre-oxidation at 800 °C in air for 500 h. Fig. 11 shows the measured ASR as a function of testing temperature for both samples. As previous studies show [1,3,5,6,8,15], it can be seen that the ASR increases with decreasing temperature and ln(ASR/T) is linearly proportional to 1/T, obeying the Arrhenius equation

$$\frac{ASR}{T} = B\exp\left(\frac{-E}{KT}\right) \tag{3}$$

where B is a pre-exponential constant, E is the activation energy, and K is the Boltzmann's constant.

In the temperature range of 550–800 °C, the ASR reduced from 22.2 to 11.5 mΩ cm^2 for the coated specimen, which is lower than that of the uncoated alloy (33.2–20.2 mΩ cm^2). This clearly demonstrates the effect of applied coating on both retarding formation of less conductive oxides, and formation of Cu–Co spinel, which has higher electrical conductivity and TEC compatibility with other SOFC components.

4. Conclusion

For the first time, the $CuCo_2O_4$ was successfully coated on the AISI 430 by sol–gel process and the performance of the coating was evaluated in air at 800 °C as a protective barrier to oxidation for the AISI 430 alloy as a metallic interconnect material of the intermediate temperature SOFCs.

The electrical conductivity and TEC of the $CuCo_2O_4$ spinel were measured in air at typical SOFC operating temperatures. These results suggest that $CuCo_2O_4$ is a potential protective coating spinel for the Cr_2O_3-forming stainless steel interconnects.

$CuCo_2O_4$ protective coating can significantly increase the oxidation resistance of the AISI 430 alloy by limiting the access of O_2 in air to the outwardly diffused cations. The parabolic rate constant of the oxidation kinetics is 5.8×10^{-13} $gr^2\ cm^{-4}\ s^{-1}$ for the coated specimen, in comparison with 3.6×10^{-11} $gr^2\ cm^{-4}\ s^{-1}$ of the uncoated.

The ASR is significantly lowered by the application of a $CuCo_2O_4$ coating, which is attributed to the thin thickness of an electrically resistive Cr_2O_3 layer (about 4 μm) and the formation of electrically conductive Cu–Co spinel in the oxide scale.

References

[1] D.R. Ou, M. Cheng, X.-L. Wang, J. Power Sources 236 (2013) 200–206.
[2] B. Hua, J. Pu, W. Gong, J. Zhang, F. Lu, L. Jian, J. Power Sources 185 (2008) 419–422.
[3] B. Hua, W. Zhang, J. Wu, J. Pu, B. Chi, L. Jian, J. Power Sources 195 (2010) 7375–7379.
[4] A. Heidarpour, G.M. Choi, M.H. Abbasi, A. Saidi, J. Alloys Compd. 512 (2012) 156–159.
[5] H. Ebrahimifar, M. Zandrahimi, Surf. Coat. Technol. 206 (2011) 75–81.
[6] A.M. Dayaghi, M. Askari, P. Gannon, Surf. Coat. Technol. 206 (2012) 3495–3500.
[7] X. Xin, S. Wang, Q. Zhu, Y. Xu, T. Wen, Electrochem. Commun. 12 (2010) 40–43.
[8] H. Rashtchi, M.A. Faghihi, A.M. Dayaghi, Ceram. Int. 39 (2013) 8123–8131.
[9] Z.H. Bi, J.H. Zhu, J.L. Batey, J. Power Sources 195 (2010) 3605–3611.
[10] N. Shaigan, W. Qu, D.G. Ivey, W. Chen, J. Power Sources 195 (2010) 1529–1542.
[11] J. Wu, C.D. Johnson, Y. Jiang, R.S. Gemmen, X. Liu, Electrochim. Acta 54 (2008) 793–800.
[12] W. Qu, J. Li, D.G. Ivey, J. Power Sources 138 (2004) 162–173.

[13] N. Shaigan, D.G. Ivey, W. Chen, J. Power Sources 183 (2008) 651–659.
[14] C.-L. Chu, J.-Y. Wang, S. Lee, Int. J. Hydrogen Energy 33 (2008) 2536–2546.
[15] C. Lee, J. Bae, Thin Solid Films 516 (2008) 6432–6437.
[16] J.H. Zhu, Y. Zhang, A. Basu, Z.G. Lu, M. Paranthaman, D.F. Lee, E.A. Payzant, Surf. Coat. Technol. 177 (2004) 65–72.
[17] S. Lee, C.-L. Chu, M.-J. Tsai, J. Lee, App. Surf. Sci. 256 (2010) 1817–1824.
[18] E.A. Lee, S. Lee, H.J. Hwang, J.-W. Moon, J. Power Sources 157 (2006) 709–713.
[19] Z. Yang, G.-G. Xia, X.-H. Li, J.W. Stevenson, Int. J. Hydrogen Energy 32 (2007) 3648–3654.
[20] W. Zhang, J. Pu, B. Chi, L. Jian, J. Power Sources 196 (2011) 5591–5594.
[21] Y. Xu, Z. Wen, S. Wang, T. Wen, Solid State Ionics 192 (2011) 561–564.
[22] A. Petric, H. Ling, J. Am. Ceram. Soc. 90 (2007) 1515–1520.
[23] N. Shaigan, D.G. Ivey, W. Chen, J. Power Sources 185 (2008) 331–337.
[24] K. Taneichi, T. Narushima, Y. Iguchi, C. Ouchi, Mater. Trans. 47 (2006) 2540–2546.
[25] M.P. Manahan, J. Mater. Sci. 25 (1990) 3424–3428.
[26] J.-H. Kim, R.-H. Song, S.-H. Hyun, Solid State Ionics 174 (2004) 185–191.
[27] T. Brylewskia, J. Dabeka, K. Przybylskia, J. Morgielb, M. Rekas, J. Power Sources 208 (2012) 86–95.
[28] Y. Fang, C. Wu, X. Duan, S. Wang, Y. Chen, Int. J. Hydrogen Energy 36 (2011) 5611–5616.